ELSEVIER

International Journal of Heat and Fluid Flow 23 (2002) 81–91

International Journal of HEAT AND FLUID FLOW

www.elsevier.com/locate/ijhff

Boundary condition effects on the flow stability in a toroidal thermosyphon

Yu Yan Jiang [a,*], Masahiro Shoji [a,1], Masashi Naruse [b,2]

[a] *Department of Mechanical Engineering, Faculty of Engineering, The University of Tokyo, 7-3-1 Hongo, Bunkyo-ku, Tokyo 113-8656, Japan*
[b] *Mitsubishi Electric Corporation, Nagoya Works, 1-14 Yada-Minami 5-Chome, Higashi-ku, Nagoya 461-8670, Japan*

Received 19 September 2000; accepted 9 October 2001

Abstract

The toroidal thermosyphon is widely used in solar water systems, nuclear reactors and geothermal energy systems, etc. The flow stability has been the main research topic but little attention was paid to the influence of boundary conditions. An experiment was performed on a copper torus. The Lorenz-like chaotic flow was not observed in clear contrast to that in the usual glass torus. Numerical simulation showed that the axial heat conduction in the tube wall deformed the heat flux distribution. A one-dimensional model generally formulated the boundary condition effects on the Hopf bifurcation. The model suggested that the metal wall could efficiently eliminate temperature perturbation, decrease the driving force and hence stabilize the global flow. The model was also used to analyze the effect of torus tilt angle on flow stability, whose conclusion agreed with previous experiment.

Keywords: Thermosyphon; Natural circulation loop; Flow stability; Lorenz model; Chaos thermal convection

1. Introduction

The natural convection in a toroidal loop has been widely studied in the last several decades, because of its applications in solar water systems, nuclear reactors and geothermal energy systems, etc. Another driving force for the wide studies has been its special situation in nonlinear dynamics, that is, a typical pedagogical example described by the Lorenz model. The liquid flow along the loop, which is placed in a vertical plane, is driven by buoyancy due to a negative vertical temperature gradient formed by heating from below and cooling from above. In spite of the simplicity of the geometry, the fluid motions and dynamic properties vary quite complicatedly and hence have not been satisfactorily formulated so far. Those researches pioneered by Keller (1966), Welander (1967), and Malkus (1972) were reviewed by Greif (1988).

Creveling et al. (1975) observed firstly the Lorenz-like chaotic flow (aperiodic flow with successive direction alternation) in their experiment. The totus tube was made of Pyrex glass. The bottom half was heated at uniform heat flux while the upper half was cooled at constant temperature (we refer to the boundary conditions as BC–QT below). The works concerning the physical mechanism include those of Malkus (1972), Hart (1984), Sen et al. (1985), Gorman et al. (1986), Yorke et al. (1987), Stern et al. (1988) and Widmann et al. (1989), etc., who applied the Lorenz model and modified it to consider various effects under the basic assumption of one-dimensionality.

However, Suda and Mimura (1989), Ehrhard and Muller (1990) and Sano (1991a) reported different experiments. Although their loops were also made of Pyrex glass the boundary conditions were different from BC–QT. In Suda and Mimura (1989) and Ehrhard and Muller (1990) the bottom half of the loops were heated at constant temperature instead of uniform heat flux (we refer to this as BC–TT). The Lorenz-like chaos was obviously delayed. In Sano (1991a) only the upper and

* Corresponding author. Tel./fax: +81-3-5841-6408.
E-mail addresses: yyjiang@photon.t.u-tokyo.ac.jp (Y.Y. Jiang), shoji@photon.t.u-tokyo.ac.jp (M. Shoji), tt76186@a1.sci.ne.jp (M. Naruse).
[1] Tel./fax: +81-3-5841-6406.
[2] Tel.: +81-52-796-2789.

0142-727X/02/$ - see front matter
PII: S0142-727X(01)00141-2

Nomenclature

Bi	Biot mumber, hd_i/k_w
c	fluid heat capacity, J/(kg °C)
d	torus tube diameter, m
g	gravity acceleration, m/s^2
h	heat transfer coefficient, W/(m^2 °C)
k	heat conductivity, W/(m^2 °C)
K	coefficient in Eq. (14)
Nu	Nusselt number, hd_i/k_f
Pr	Prandtl number
q	heat flux, W/m^2
$r, \varphi, \theta, r_o, r_i$	coordinates and variables defined in Fig. 3
R	main radius of the torus, m
Ra	Rayleigh number
Re	Reynolds number
t	time, s
T	temperature, °C
T_3, T_6, T_9	bulk temperature of the fluid in the places shown in Fig. 1, °C
w	fluid velocity along the pipe, m/s

Greeks

α	tilt angle of the torus
β	thermal expansion coefficient, K^{-1}
λ	eigenvalue of coefficient matrix
Φ	superheat
μ	dynamic viscosity of fluid, kg/(m s)
ρ	density of the fluid, kg/m^3
σ	$16Pr\ Nu^{-1}$
τ_w	shear stress, kg/(m s^2)

Subscripts

b	bulk flow
c	cooling, reference value
E	even mode
f	fluid
h	heating
i	inner tube surface
in	the entrance of heating section
o	outer tube surface
O	odd mode
out	the entrance of heating section
q	uniform heat flux boundary condition
T	constant temperature wall boundary condition
w	tube wall

bottom quarters of the torus were cooled/heated at constant temperatures. The Lorenz-like chaos did not appear ($Ra/Ra_c = 298.9$). They attributed the difference of results to local three-dimensional flow disturbance, which changed the overall friction losses and reduced the buoyancy by leveling out temperature gradients. Sano (1991a,b) proposed a three-dimensional model, which successfully formulated the intermittence bifurcation to chaos.

In engineering practice thermosyphon systems are made of metal materials due to the better processing properties and higher thermal conductivity. We built a torus to study the wall effects on natural convection. Although its shape and boundary conditions were the same as those in Creveling et al. (1975) the torus was made of copper instead of glass. The Lorenz-like chaotic flow never appeared. The discrepancies between the above-mentioned experiments imply that the boundary conditions and the tube wall material crucially affect the flow behavior in the toroidal thermosyphon.

2. Experimental study

2.1. Experimental setup

The torus of the thermosyphon (see Fig. 1) was fabricated from two 23 mm inner diameter pure copper

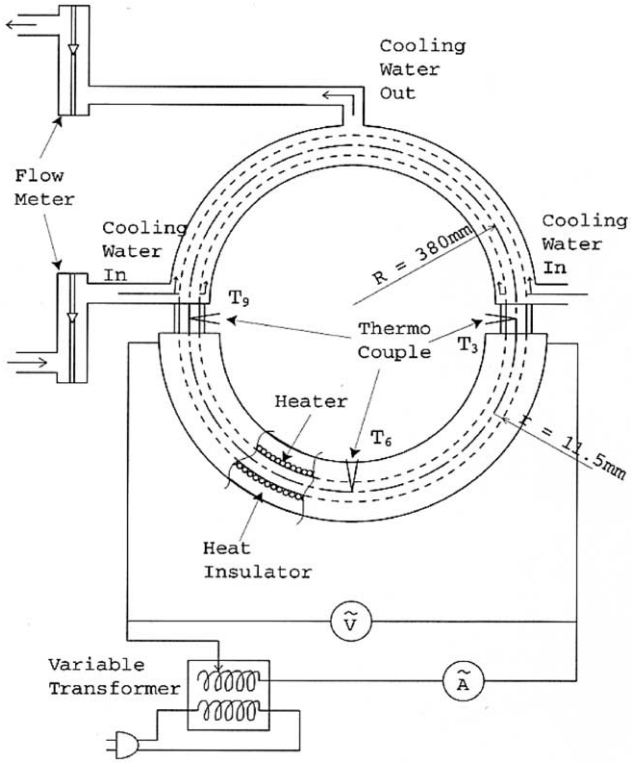

Fig. 1. Toroidal thermosyphon experimental setup.

tube halves with a main radius of $R = 380$ mm. The tube thickness was 1.25 mm. Two sections of 62 mm long Plexiglas with the same inner diameter connected the copper sections for the visualization, the thermal expansion and the temperature measuring. The sections introduced no considerable effects on the friction property of the system.

The torus was cooled by means of a water jacket, which surrounded the upper half portion. The water jacket was made of copper tube section in 34 mm inner diameter. The cooling tap water flew into the jacket at a flow rate larger than 2 l/min, which kept the wall temperature T_w always constant. The lower half was heated with 5 SIL 10206 type linear heaters that were evenly wound around the tube and were connected in parallel with a RSD 10A transformer. The heaters' resistances were 47.98, 48.39, 48.03, 49.39, and 49.06 Ω from left to right. The rated power of the transformer was 1300 VA. The heated section was covered with multi-layers of fiberglass blanket approximately 13 mm thick. That insulation method assured that heat loss was less than 1% of the generated heat.

Temperatures were measured by T-type thermocouples. A TR6841 digital recorder measured the heating power. A TR7200 digital scanner scanned the measured signals; while a YEW 3056 pen recorder plotted the fluid temperatures T_3, T_6, T_9 simultaneously. An SVX-485DX2 PC controlled the scanner and accumulated the measured data. A small amount of Polystyrene latex micro particles was seeded in the fluid to visualize the flow.

At each run the heating power increased directly from zero to the specialized value. The symmetric of the heating and cooling sections to the vertical axis was examined. The flow could be clockwise or anti-clockwise by chance. The measurement time was longer than 3 h, which was long enough for recording all typical flow behavior that may appear.

2.2. Results and discussion

The working fluid in the thermosyphon tube was distilled water. Following the ideas of previous researchers (Creveling et al., 1975; Gorman et al., 1986, etc.), the time series of T_9, T_6 and T_3 could tell the story of the flow features. The oscillation of $T_3 - T_9$ represented the vibration of flow speed. Let T_{in} and T_{out} represent the temperatures at the entrance and the exit to the heating section. If $T_3 - T_9 > 0$, the flow was counterclockwise, and $T_{in} = T_9$, $T_{out} = T_3$, else, the flow was clockwise, and $T_{in} = T_3$, $T_{out} = T_9$. That relation was verified by visual observation. Table 1 shows the ranges of the following different flow motions reflected by temperatures under heating powers of approximately $q = 0.006$–1.39 W/cm^2 (5–1200 W).

2.2.1. Steady flow (see Fig. 2(1))

The liquid began flowing at the smallest heating power (5 W). The flow was steady without undergoing any oscillatory process when the heat flux was less than 0.012 W/cm^2. With increase in the heating power, T_9 and T_3 underwent a short time of oscillation before becoming stable, which implied that the unbalances of the temperature field increased. However, the temperature in the bottom T_6 had no oscillation at all until the heat flux reached 0.023 W/cm^2.

2.2.2. Periodically oscillatory flow (see Fig. 2(2))

At a heat flux of 0.023 W/cm^2, T_{out} began to oscillate periodically with constant amplitude at first. T_{in} and T_6 showed also the oscillation at 0.052 W/cm^2 and 0.087 W/cm^2, respectively. In contrast, the oscillation amplitudes of T_{in} and T_6 were much smaller than that of T_9, which suggested the perturbations caused by heating were large. T_6 oscillated with one or two base frequencies until the heating power was increased very large. For instance, Fig. 2(2) shows the power spectrum of $T_3 - T_9$ at $q = 0.058$ W/cm^2, where the unique base frequency was detected. The number of base frequencies increased along with the heating power until no apparent base frequencies were distinguished at 0.070 W/cm^2. The base frequency (0.006–0.1 Hz) is equivalent to that of the liquid flowing a circle, which means that the complexity of T_3 and T_9's variation might result from the complicated alternation between the hot and cool liquid in the heating–cooling connections (Sano, 1991b).

Table 1
The heat flux q scopes of different flow motions

Terms	q (W/m^2)			
	Stable state		Periodic oscillation state	Chaotic oscillation state[a]
	With stable starting process	With oscillatory starting process		
T_{out}	0.006–0.012	0.012–0.023	0.023–0.070	0.070
T_6	0.006–0.023	0.023–0.087	0.087–0.695	0.695
T_{in}	0.006–0.012	0.012–0.052	0.052–0.064	0.064
$T_3 - T_9$ ($T_{out} - T_{in}$)	0.006–0.012	0.012–0.023	0.023–0.064	0.064

[a] The upper range of the chaotic oscillation state is limited by the largest heating power of our experiment.

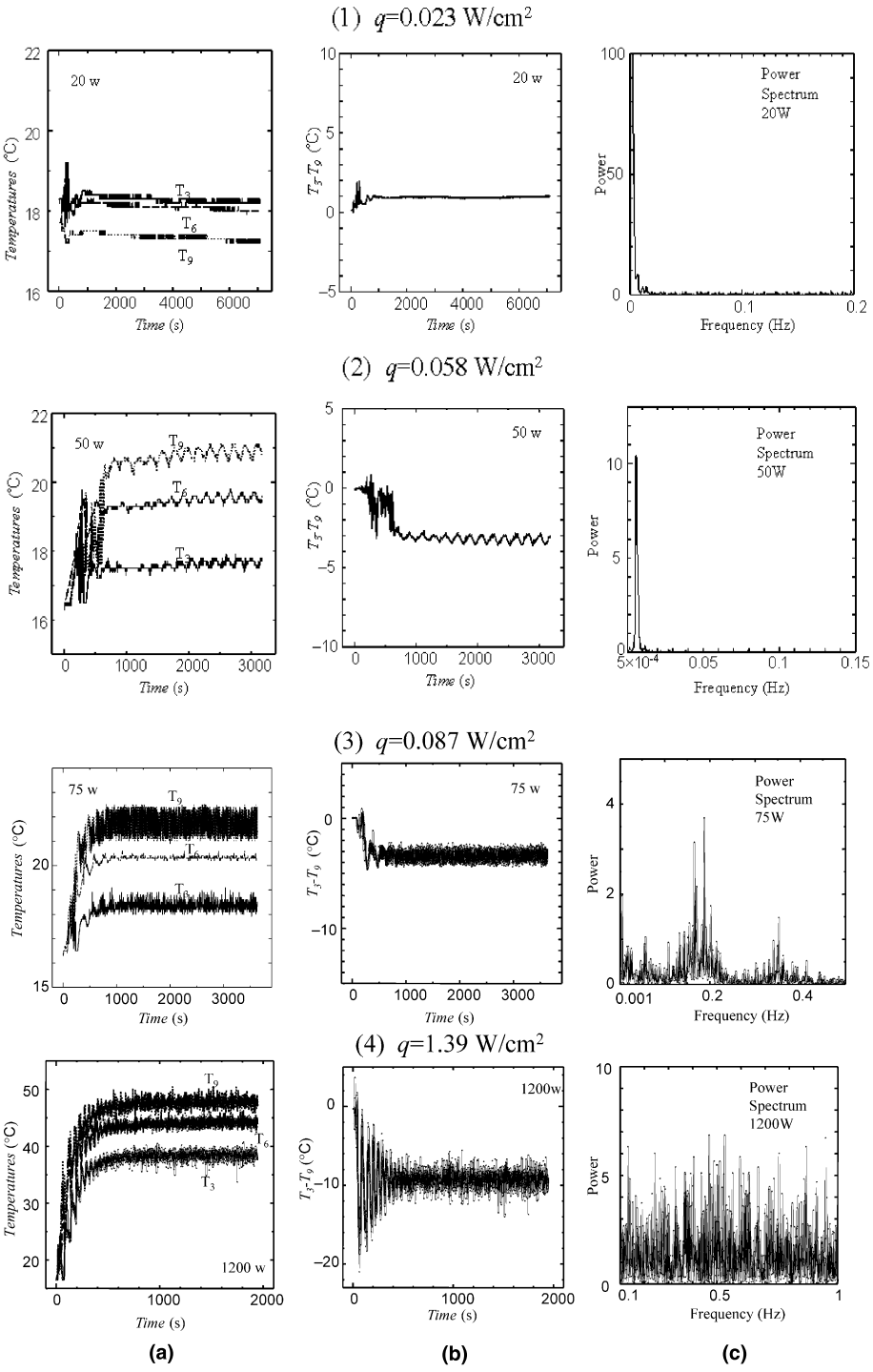

Fig. 2. Some typical experimental results at different heating powers. (a) Time series of T_3, T_6 and T_9. (b) Time series of $T_3 - T_9$. (c) Power spectrum of $T_3 - T_9$ at normal operating states.

2.2.3. Chaotically oscillatory flow (see Fig. 2(3)–(4))

The oscillations of the three temperatures became chaotic at last as the heating power increased, where the amplitudes also increased with the heating power. However, amplitudes always remained at constant value when the starting process was finished. Within the limitation of the present heating power, no Lorenz-like chaos was observed. The flow did not change directions no matter what kind of starting method was tried (other methods such as increasing the heating power to the specialized value step by step or decreasing it to the specialized value from the largest, were also tried). The flow velocity was approximated by the base frequency of flow oscillation and energy conservation based on the

values of q and $T_3 - T_9$. Both suggested the flow was already in turbulence regime ($Re \approx 2500$).

The only difference between the present experimental rig and that in Creveling et al. (1975) was the tube wall, which brought out the different results. The numerical simulation in Section 3 demonstrates the effect of tube wall.

3. Numerical investigation

Careful analysis of Fig. 2 shows that the relation $|\overline{T_{in} - T_6}| > |\overline{T_{out} - T_6}|$ always exists no matter whether the flow is clockwise or counter-clockwise. The relation suggests that heat is mainly transferred through the entrance quarter, which violates the uniform heat flux assumption. In fact, the wall temperature and heat flux distributions inside are quite different from those outside, which can be investigated by numerical simulation.

Fig. 3 shows the coordinate system. Suppose the bottom half ($\pi < \theta < 2\pi$) is heated with uniform heat flux q (BC–QT) or at constant temperature T_h (BC–TT). The liquid temperature is T_b. The flow velocity w is supposed to be anti-clockwise. Let the characteristic length be d_i and the superheat be $\Phi = (T - T_c)/(q/h)$ for BC–QT and be $\Phi = (T - T_c)/(T_h - T_c)$ for BC–TT, where h is the heat transfer coefficient between liquid and wall. The dimensionless steady state heat conduction equation of the tube wall is expressed as follows.

The dimensionless steady state heat conduction equation of the tube wall is

$$\frac{\partial}{\partial r}\left[(R + r\cos\varphi) r \frac{\partial \Phi}{\partial r}\right] + \frac{1}{r}\frac{\partial}{\partial \varphi}\left[(R + r\cos\varphi)\frac{\partial \Phi}{\partial \varphi}\right] + \frac{r}{R + r\cos\varphi}\frac{\partial^2 \Phi}{\partial \theta^2} = 0. \quad (1)$$

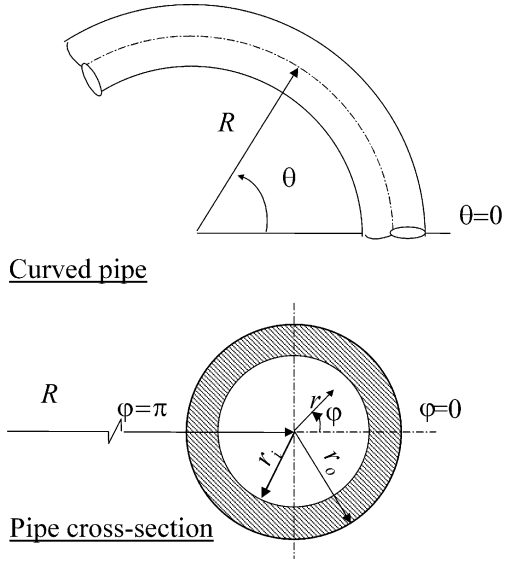

Fig. 3. The toroidal coordinate system.

The boundary conditions for the bottom half are:

(i) inner surface, convection with fluid:

$$r = r_i = 0.5, \quad \frac{\partial \Phi}{\partial r} = \frac{h d_i}{k_w}(\Phi_w - \Phi_b) = Bi(\Phi_w - \Phi_b);$$

(ii) outer surface, uniform heat flux:

$$r = r_o, \quad \frac{\partial \Phi}{\partial r} = \frac{q d_i}{k_w T_c} = Bi\frac{q}{h T_c},$$

or constant wall temperature: $r = r_o$, $\Phi = 1$;

(iii) insulated at both ends:

$$\left.\frac{\partial \Phi}{\partial \theta}\right|_{\theta=\pi,2\pi} = 0;$$

(iv) symmetry about the plane:

$$\Phi = 0, \pi: \quad \left.\frac{\partial \Phi}{\partial \varphi}\right|_{\varphi=0,\pi} = 0.$$

The bulk fluid temperature T_b is calculated from the energy conservation between the heat absorbed by the liquid and that entering the control volume, so that

$$\rho_f c \pi r_i^2 w d T_b = 2\pi r_i h (T_w - T_b)\cdot(R + r)\,d\theta, \quad (2)$$

where ρ_f and c are the fluid density and heat capacity. By integration from π to θ, Eq. (2) becomes dimensionless, or,

$$\Phi_b = \frac{\theta - \pi}{\rho_f c r_i w/2h(R + r_i) + \theta - \pi}\Phi_w, \quad (3)$$

where Φ_b and Φ_w were determined by iterative calculation. According to the real experimental setup, the following values are assumed: $d_o/d_i = 1.1$, $R/d_i = 16$, $Bi = 0.1$ for copper tube and 35 for glass tube, and $\rho_f c r_i w/2h(R + r_i) = 0.5$.

The equation was numerically solved by finite difference method in FORTRAN. Fig. 4 shows the results. In the tube with small heat conductivity, Fig. 4(1) shows that the heat fluxes uniformly distribute both on outer and inner surfaces. Both the temperatures of the wall and the fluid increase linearly along the loop. The boundary condition of uniform heat flux remains unchanged. However, in the tube with large heat conductivity, Fig. 4(2) shows that the heat flux distribution is deformed. The axial heat conduction eliminates the axial (θ) temperature gradients. As a result, the heat is mainly transported through the entrance quarter, and the wall temperature seems axially constant. The wall axial heat conduction is responsible for the relation of

$$\left|\overline{T_{in} - T_6}\right| > \left|\overline{T_{out} - T_6}\right|$$

in the present experiment. Similarly, if the bottom half with small heat conductivity is at constant temperature, Fig. 4(3) shows that the temperature distribution also varies spatially. The wall temperature in the inner surface changes with fluid because the axial heat conduction in the wall is faint.

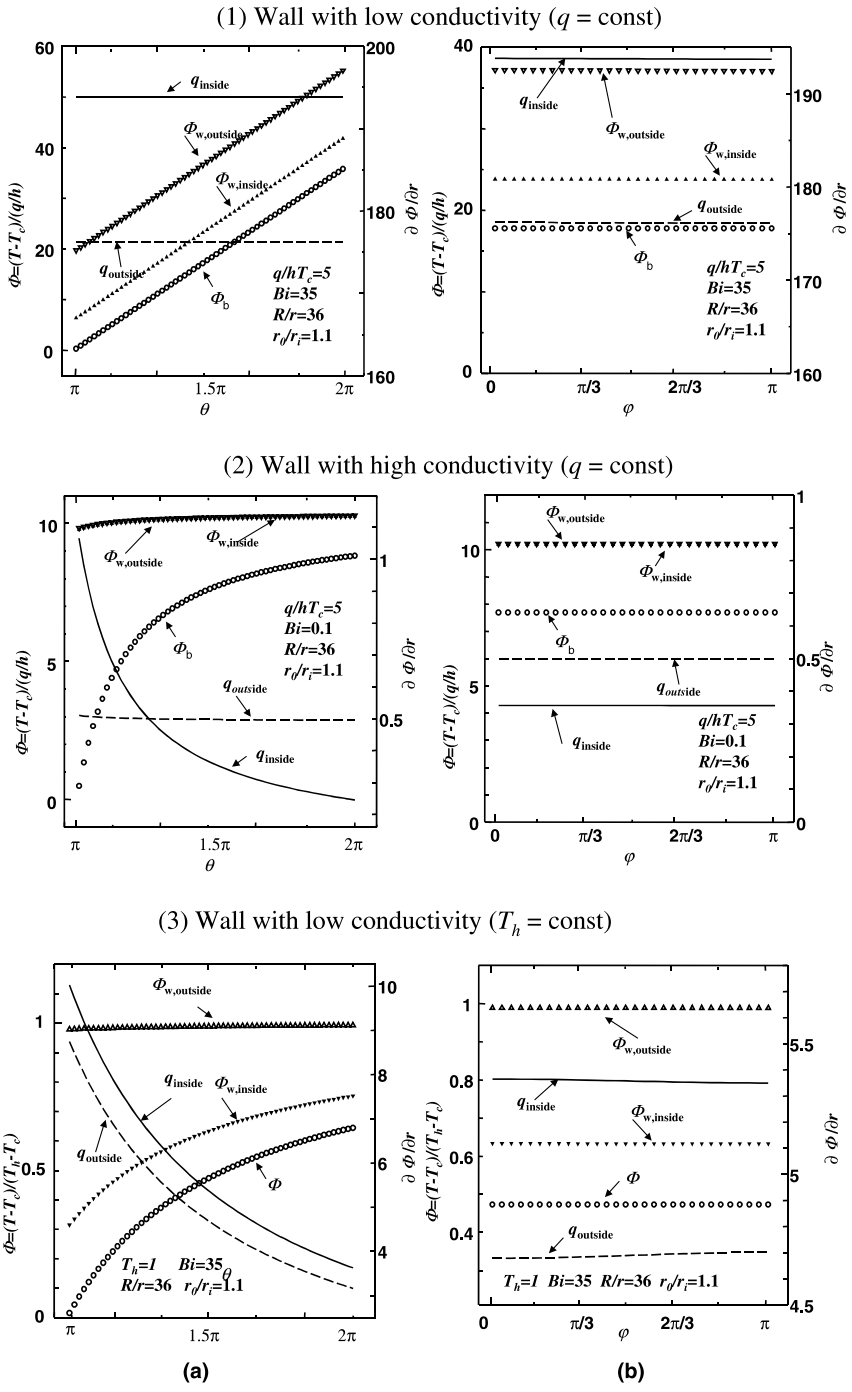

Fig. 4. Temperatures and heat fluxes in/outside tube walls: (a) arial distribution ($\varphi = 0$); (b) peripheral distribution ($\theta = 3\pi/2$).

Fig. 4 implies that the tube wall affects intensively the real boundary conditions and hence flow behavior. In fact Ehrhard and Muller (1990) drew a similar conclusion when they considered the influence of liquid–wall property on flow behavior. They also suggested that the wall with high heat conductivity has advantages for stabilizing the global flow. The one-dimensional model in the next section will show the mechanism.

4. One-dimensional modeling of the boundary condition effects

The spontaneous chaos appears through two approaches as soon as the loop flow is laminar. The first one is Hopf bifurcation and catastrophe of global flow, which leads to the Lorenz-like chaos. The second one is intermittence bifurcation of local sub-harmonic waves, which leads to cellular flow. In a real system both ten-

dencies exist simultaneously and restrict each other. The critical values of control parameter determine which bifurcation will finally happen. The flow bifurcation in our loop exhibited some features of the latter, which was well formulated by Sano (1991a,b) in his three-dimensional model. However, we need not build another Sano-like model because we aim to formulate, if any, the boundary condition influence on the Hopf bifurcation.

The one-dimensional features of the flow are ensured by three facts. Firstly, the secondary flows decrease the spatial temperature and velocity gradients in θ cross-sections. Secondly, the fluid Prandtl number is large ($Pr > 1$), which makes the momentum transported more efficiently than the energy (Gorman et al., 1986). Thirdly, the truncation of the fluid temperature Fourier series expansion brings out a little discrepancy (Yorke et al., 1987). Since Fig. 4(1) showed that the fluid is really under BC–TT in our experiment, we examine the discrepancy between BC–TT and BC–QT at first. After that we generalize the model to other boundary conditions.

4.1. Boundary conditions of BC–TT

Following Gorman et al. (1986), we consider a loop heated at constant temperature T_h, over the bottom half and cooled at constant temperature T_c, over the top half. Consider an infinitesimal cylindrical control volume of fluid in the loop, with volume $\pi r_o^2 R\,d\theta$. Assuming incompressible plug flow, the velocity of the control volume is $w(t)$. The momentum is $\pi r_o^2 R\,d\theta \cdot \rho w(t)$; the total force on the fluid element is $\rho\pi r_o^2 R\,d\theta\frac{dw}{dt}$; the force due to the pressure gradient is $-\pi r_o^2 R\,d\theta\frac{dP}{d\theta}$; the body force term due to gravity is $\rho g\pi r_o^2 R\cos\theta\,d\theta$; and the shear force at the wall of the tube is $-\tau_w 2\pi r_o R\,d\theta$, where $\tau_w = 8\rho_f w^2/Re$ is the shear stress in laminar flow. The momentum equation for the fluid is therefore

$$\rho\pi r_o^2 R\,d\theta\frac{dw}{dt} = -\pi r_o^2 d\theta\frac{dP}{d\theta} - \rho g\pi r_o^2 R\,d\theta\cos\theta - \tau_w 2\pi r_o^2 R\,d\theta. \tag{4}$$

Let the density of the fluid be given by $\rho = \rho_c[1-\beta(T-T_c)]$, where β is the thermal expansion coefficient of the fluid. In the Boussinesq approximation, substituting the expression for ρ into the body force term, but letting $\rho = \rho_c$ in all other terms, and integrating from 0 to 2π yields,

$$\rho_c\frac{dw}{dt} = \frac{\beta\rho_c g}{2\pi}\int_0^{2\pi}(T-T_c)\cos\theta\,d\theta - \frac{2\tau_w}{r_o}. \tag{5}$$

The rate of change of thermal energy in the control volume is

$$\rho_c c\pi r_o^2 R\,d\theta\left(\frac{\partial T}{\partial t} + \frac{w}{R}\frac{\partial T}{\partial\theta}\right),$$

which must equal the amount of heat entering the control volume. The heat entering the control volume is $-2\pi r_o R\,d\theta\cdot h(T-T_c)$ in the upper half or $-2\pi r_o R\,d\theta\cdot h(T_h-T)$ in the bottom half. The energy balance equation can be written,

$$\rho_c c\left(\frac{\partial T}{\partial t} + \frac{w}{R}\frac{\partial T}{\partial\theta}\right) = \begin{cases} -2h(T-T_c)/r_o, & 0<\theta\leqslant\pi, \\ 2h(T_h-T)/r_o, & \pi<\theta\leqslant 2\pi, \end{cases} \tag{6}$$

where the heat transfer coefficient is a function of flow velocity, $h = h_0 f(w)$. The heat resistance of tube wall is included in h to consider the effect of wall property. Eqs. (5) and (6) can be made dimensionless as follows:

$$\frac{d\omega}{d\tau} + \Gamma\omega = \frac{\pi\Gamma}{4D}\int_0^{2\pi}\Phi\cos\theta\,d\theta, \tag{7}$$

$$\frac{d\Phi}{d\tau} + 2\pi\omega\frac{\partial\Phi}{\partial\theta} = \begin{cases} -2D\Phi f(\omega), & 0<\theta\leqslant\pi, \\ 2D(1-\Phi)f(\omega), & \pi<\theta\leqslant 2\pi \end{cases} \tag{8}$$

with the following transformations:

$$\Phi = \frac{T-T_c}{T_h-T_c},\quad \omega = \frac{w}{V},\quad \tau' = \frac{t}{2\pi R/V}$$

and

$$V = \left(\frac{g\beta R r_o h_0(T_h-T_c)}{2\pi c\mu}\right)^{0.5},\quad D = \frac{2\pi R h_0}{\rho_c c r_o V},$$

$$\Gamma = \frac{16\pi\mu R}{\rho_c r_o^2 V}.$$

In order to find the ordinary differential Lorenz-like equations, we expand Φ in a Fourier series, $\Phi = a_0(\tau) + \sum a_n(\tau)\cos n\theta + \sum b_n(\tau)\sin n\theta$. Multiplying the energy equation by $\cos n\theta$ and $\sin n\theta$, respectively can decouple a_n and b_n. The equations for ω, a_1 and b_1 are independent of those for the high order coefficients. These are:

$$\dot{x} = \sigma(y-x), \tag{9}$$

$$\dot{y} = -zx + Ra_T x - 2yf(x), \tag{10}$$

$$\dot{z} = xy - (2z - Ra_T)f(x), \tag{11}$$

where

$$x = \frac{2\pi\omega}{D},\quad y = \frac{\pi^3}{2D^2}a_1,\quad z = \frac{\pi^3}{2D^2}b_1 + Ra_T,\quad \tau = D\tau'$$

and

$$Ra_T = \frac{2\pi^2}{D^2} = \frac{\rho_f c^2 r_o^2}{2R^2 h_0}\cdot\frac{g\beta R r_o(T_h-T_c)}{2\pi c\mu},$$

$$\sigma = \Gamma/D = \frac{8\mu c}{r_o h_0} = \frac{16Pr}{Nu}.$$

We discuss the model comparing with that by Gorman et al. (1986). Note that both Ra_T and Ra_q are defined at steady states, at which the energy absorbed from the heating section equals that disposed into the cooling section. Suppose the heat transfer coefficient is constant, the average fluid temperature should be $\bar{T} = (T_h + T_c)/2$ at steady state, and the characteristic heat flux in the

heating half should be $q = ((T_h - T_c)/2)h_0$. Therefore, $Ra_T = 2Ra_q$, where

$$Ra_q = \frac{\rho_f c^2 r_o^2}{2R^2 h_0^2} \cdot \frac{g\beta R r_o q}{2\pi c\mu}$$

was defined by Creveling et al. (1975).

Firstly we take the heat transfer coefficient as constant, that is $f(w) = 1$, in favor of dynamical analysis. The model has three steady states, $(0, 0, Ra_T/2)$ and

$$\left[\pm (Ra_T - 4)^{0.5}, \pm (Ra_T - 4)^{0.5}, Ra_T - 2\right],$$

which stand for the static heat conduction and steady flow in clockwise (−) and anti-clockwise (+) directions. The static heat conduction state gives way to convection when $Ra_T \geqslant 4$ (saddle-node bifurcation). The flow stability can be judged by local linear analysis. The characteristic equation of the coefficient matrix in Eqs. (9)–(11) in either steady flow state is

$$\lambda^3 + (4+\sigma)\lambda^2 + (Ra_T + 2\sigma)\lambda + 2\sigma(Ra_T - 4) = 0, \quad (12)$$

which possesses one negative real and two conjugate complex solutions. The real parts of the two complex solutions become positive (the Hopf bifurcation) when the product of the coefficients of λ^2 and λ is less than the constant term, or

$$\begin{aligned} Ra_T &< 2\sigma(\sigma+8)(\sigma-4)^{-1} < 0, \quad \sigma < 4, \\ &> 2\sigma(\sigma+8)(\sigma-4)^{-1} > 0, \quad \sigma > 4. \end{aligned} \quad (13)$$

Negative Rayleigh number is meaningless. The Lorenz-like chaos could appear only if $\sigma > 4$ and $Ra_T > 2\sigma(\sigma+8)(\sigma-4)^{-1}$. In the loop under BC–QT, the model by Gorman et al. (1986) gives critical values for Hopf bifurcation as

$$Ra_q = 0.5Ra_T > \sigma(\sigma+4)(\sigma-2)^{-1}$$

and $\sigma > 2$, both of which are smaller.

Under BC–TT, the driving force (buoyancy) decreases because the heat is mainly transported through the entrance quarters as mentioned in Section 3. The fact can be indirectly reflected by the different flow variations with heating power in different loops. In Fig. 5 we compared the variation of the flow velocity in our loop with those in some references. The figure shows that the flow velocity increases linearly under BC–QT while logarithmically under BC–TT. Since the driving force is relatively smaller the critical Rayleigh number for Hopf bifurcation is postponed to a higher value. The conclusion was also drawn by Suda and Mimura (1989) and Ehrhard and Muller (1990).

Welander (1967) proved that the flow oscillation results from temperature perturbation. σ is just the measurement of the system property for temperature perturbation removed. In the system with small σ, the temperature perturbations will be efficiently removed by

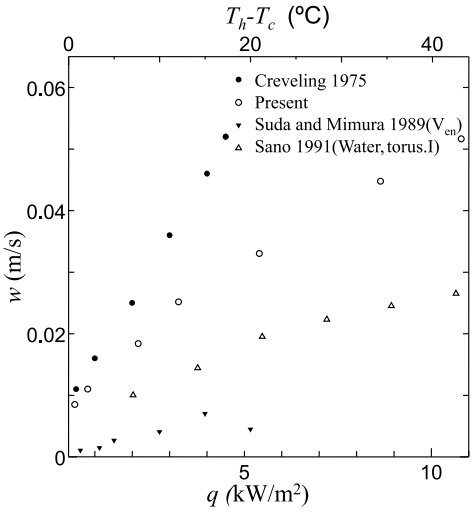

Fig. 5. Flow velocities as functions of heating power in different loops.

heat diffusion in liquid (small Pr) and/or heat exchange between liquid and wall (large Nu). The critical σ for Hopf bifurcation under BC–TT is larger than that under BC–QT because the former wall is better at temperature perturbation elimination. That is because the heat transfer between the liquid and the wall with constant temperature can effectively remove the local temperature bulge or concavity of the fluid.

The data from the present experiment shown in Fig. 6 verified the above argument. In the whole experiment, either Ra or σ was insufficient for the Hopf bifurcation and hence the global flow was always stable. The right chart in Fig. 6 shows the corresponding flow velocities, which were well predicted by the model.

In order to discuss further the effects of heat transfer property on the Hopf bifurcation, we consider the case that h increases with flow rate. Ehrhard and Muller (1990) recommended the following expression:

$$h = h_0\left(1 + K|w|^{1/3}\right) = h_0\left(1 + \frac{K}{(2Ra_T)^{1/3}}|x|^{1/3}\right). \quad (14)$$

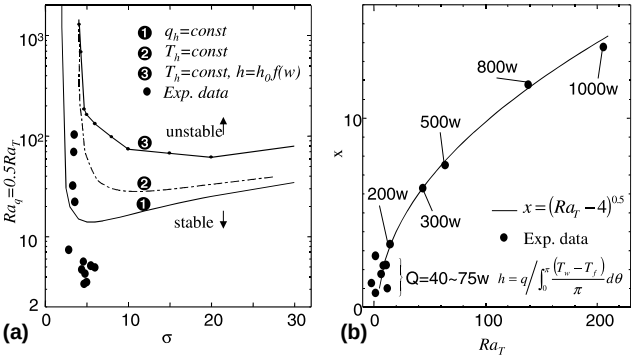

Fig. 6. Comparison of experiment and theory: (a) criteria for Hopf bifurcation of global flow and (b) measured and predicted flow rates.

The stable domain for $K = 0.3$ is plotted in Fig. 6(a) by numerical experiment data. The system becomes more stable because the temperature perturbations can be removed more efficiently at high flow rate, which agrees with the conclusion by Ehrhard and Muller (1990) (their Section 2.5).

4.2. General boundary conditions

We generally investigate the influence of boundary conditions on the Hopf bifurcation. Any boundary condition can be expressed by the axially distributed temporal heat flux $q(\theta,t)$ or temperature $T_w(\theta,t)$. Although they are equivalent, we adopt $q(\theta,t)$ rather than the wall temperature $T_w(\theta,t)$ in favor of analysis. The torus may tilt an angle of α in the vertical plane. For the flow at those boundary conditions, Eq. (5) still exists while the energy equation becomes,

$$\rho_c c\left(\frac{\partial T}{\partial t}+\frac{w}{R}\frac{\partial T}{\partial \theta}\right)=q(\theta,t)/r_o. \tag{15}$$

The Fourier expansion of $q(\theta,t)$ seems reasonable. However, the Fourier expression for the axial distribution of heat flux may temporally vary with fluid temperature (recall, for instance, that heat is mainly transported through the entrance quarters at BC–TT), or $q(\theta,t,T)$. Under an assumption that boundary conditions are axial-symmetric to the axis $\theta=\alpha+\frac{\pi}{2}$ at static heat conduction, $q(\theta,t,T)$ is cast into a Fourier series of $\theta'=\theta-\alpha-\pi/2$, that is,

$$\begin{aligned} q &= O_0' + \sum_1 O_n(T,t)\cos n\lfloor\theta-(\pi/2+\alpha)\rfloor \\ &\quad + \sum_1 E_n(T,t)\sin n\lfloor\theta-(\pi/2+\alpha)\rfloor \\ &= q_0[O_0(T,t)+O(T,t)\sin(\theta-\alpha)+E(T,t)\cos(\theta-\alpha)] \\ &\quad + \sum_2 O_n(T,t)\cos n[\theta-(\pi/2+\alpha)] \\ &\quad + \sum_2 E_n(T,t)\sin n[\theta-(\pi/2+\alpha)], \end{aligned} \tag{16}$$

where q_0 represents the average heat flux. Following the procedure in Section 4.1, the fluid temperature is expanded as a Fourier series of $\theta-\alpha$,

$$\Phi = a_0 + \sum a_n\cos n(\theta-\alpha)+\sum b_n\sin n(\theta-\alpha),$$

where $\Phi=(T-T_c)/(q_0/h_0)$. We cast Eq. (5) and Eq. (15) into ordinary differential equations. The equations for the first four base modes are independent of those for the other high modes, or

$$\dot{a}_0 = 2O_0, \tag{17}$$

$$\dot{x} = \sigma(y\cos\alpha - z\sin\alpha - x), \tag{18}$$

$$\dot{y} = -zx + Ra_q x + \frac{\pi}{2}Ra_q E, \tag{19}$$

$$\dot{z} = xy + \frac{\pi}{2}Ra_q O, \tag{20}$$

where w, a_1, a_2 were transformed into x, y, z as described in Section 4.1, but

$$V=\left(\frac{g\beta R r_o q_0}{2\pi c\mu}\right)^{0.5}$$

and

$$Ra_q=\frac{2\pi^2}{D^2}=\frac{\rho_f c^2 r_o^2}{2R^2h_0^2}\cdot\frac{g\beta R r_o q_0}{2\pi c\mu}.$$

Eq. (17) suggests that the average heat flux only acts on the average fluid temperature but not on the flow behavior. E and O only act on y and z directly. We assume that,

$$\frac{\pi}{2}Ra_q E = C_E y \quad\text{and}\quad \frac{\pi}{2}Ra_q O = C_O z + C_{Ra}Ra_q \tag{21}$$

so as to simplify the analysis. Here, $C_E = C_O = -1$, $C_{Ra}=0$ corresponds BC–QT, $C_E = C_O = -2$, $C_{Ra}=1$ corresponds BC–TT.

Under symmetric BC–QT ($\alpha=0$), Widmann et al. (1989) observed that the Lorenz-like chaos disappears due to the flow transition from laminar to turbulent, which was attributed to the sudden change of friction. However, the case of asymmetric BC–QT ($\alpha\neq 0$) seems different. Damerell and Schoenhals (1979) drew, using the experimental data, a Rayleigh number scope for Lorenz-like flow as a function of α, where the scope narrowed with α until disappearing at $\alpha=\pm 6°$. For asymmetric BC–TT, the experiments in Ehrhard and Muller (1990) recorded no Lorenz-like flow in the torus, although their one-dimensional model had predicted it. They attributed this contradiction to the increased dissipative effects of the local three-dimensional flow disturbances occurring with higher intensity at higher values of the heating rate. However, the explanation seems not adequate. The numerical results of Lavine et al. (1986) displayed the decreased local flow reversals at increased tilt angle, which was well reasoned in their paper.

In fact, we also drew a similar chart for Lorenz-like flow under BC–QT and BC–TT (see Fig. 7). As soon as the flow is laminar (expression for friction unchanged), the Lorenz-like chaos never disappears if $\alpha=0$, but it does if $\alpha\neq 0$. The Hopf bifurcation is more sensitive for tilt angle under BC–TT ($\alpha<\pm 1.625°$) than under BC–QT ($\alpha<\pm 10.75°$). If the parameter Ra is higher than the scope, the system will undergo a procedure like the transient-chaos recorded by Gorman et al. (1986). The orbit experiences aperiodically direction alternations for a while and then is captured by the steady flow in the direction that the torus tilted. The steady flow in the other direction seems non-absorbing. The physical mechanism needs further research.

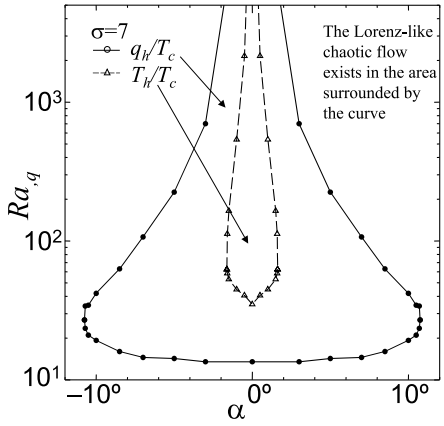

Fig. 7. *Ra* scope for Lorenz-like flow as a function of tilt angle.

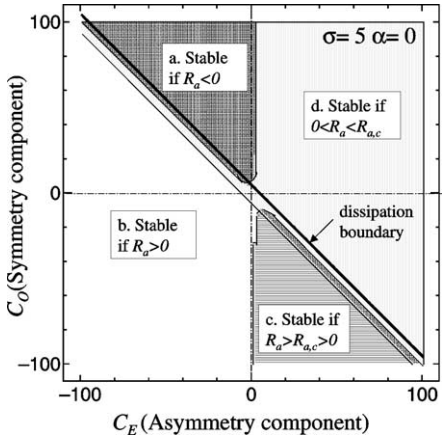

Fig. 8. *Ra* domains of stable flow varying with boundary conditions.

Finally we consider the general boundary conditions without tilt angle. Fig. 8 shows boundary condition domains of four types of flow bifurcations, which was drawn by numerical experiments at $\sigma = 5$. In regions (a) and (d) the Lorenz-like flow appears if *Ra* becomes larger than a critical value. In contrast the Lorenz-like flow exists only if *Ra* is less than a critical value in regions (b) and (c). BC–QT and BC–TT lie in region (d). The figure implies that negative C_E and C_O are favorable for stable flow. Negative C_E means heat is mainly transported through the entrance quarters, and negative C_O represents heating from bottom and cooling from above. The area above the dissipation boundary line ($C_E + C_O - \sigma > 0$) is meaningless in the physical sense because the system becomes non-dissipative.

5. Conclusions

We did an experiment on a toroidal thermosyphon fabricated from copper tube. The natural convection was in clear contrast to that in the usual glass torus. The Lorenz-like chaotic flow was not observed. A one-dimensional model was proposed to formulate the boundary condition influence on the Hopf bifurcation. Main conclusions were drawn as follows.

1. The axial heat conduction in the tube wall deforms the heat flux distribution and hence affects the global flow stability.
2. The one-dimensional model provides threshold values of control parameters for the Hopf bifurcation. The metal tube can stabilize the natural convection due to two reasons. Firstly, the heat is mainly transported through entrance section, which decreases the whole driving force (buoyancy). Secondly, the better heat transfer property eliminates temperature perturbations more efficiently.
3. The torus tilt angle affects greatly the flow behavior as well. The Hopf bifurcation can only take place at very small tilt angle. The predictions were verified by previous experiment (Damerell and Schoenhals, 1979).

References

Creveling, H.F., Depaz, J.F., Baladi, J.Y., Schoenhals, R.J., 1975. Stability characteristics of a single-phase convection loop. J. Fluid Mech. 67, 65–84.

Damerell, P.S., Schoenhals, R.J., 1979. Flow in a toroidal thermosyphon with angular displacement of heat and cooled sections. ASME J. Heat Transfer 101, 672–676.

Ehrhard, P., Muller, U., 1990. Dynamical behaviour of natural convection in a single-phase loop. J. Fluid Mech. 217, 487–518.

Gorman, M., Widmann, P.J., Robbins, K.A., 1986. Nonlinear dynamics of convection loop: a quantitative comparison of experiment with theory. Phys. D 19, 255–267.

Greif, R., 1988. Natural circulation loops. J. Heat Trans-T ASME 110, 1243–1258.

Hart, J.E., 1984. A new analysis of a closed loop thermosyphon. Int. J. Heat Mass Transfer 27, 125–136.

Keller, J.B., 1966. Periodic oscillations in a model of thermal convection. J. Fluid Mech. 26, 599–606.

Lavine, A.S., Greif, R., Humphrey, J., 1986. 3-Dimensional analysis of natural-convection in a toroidal loop-effect of tilt angle. J. Heat Trans-T ASME 108, 796–805.

Malkus, W.R.V., 1972. Non-periodic convection at high and low prandtl number. Mem., Soc., R. Sci. Liege 4kk, 125–128.

Sano, O., 1991a. Cellular structure in a natural convection loop and its chaotic behavior, 1: experiment. Fluid Dyn. Res. 8, 189–204.

Sano, O., 1991b. Cellular structure in a natural convection loop and its chaotic behavior, 2: theory. Fluid Dyn. Res. 8, 205–220.

Sen, M., Ramos, E., Trevino, C., 1985. On the steady state velocity of the inclined toroidal thermosyphon. ASME J. Heat Transfer 107, 974–977.

Stern, C.H., Greif, R., Humphrey, J., 1988. An experimental-study of natural-convection in a toroidal loop. J. Heat Transfer-T ASME 107, 877–884.

Suda, F., Mimura, K., 1989. Temperature and velocity distribution in a circular natural convection loop. In: The 26th National Heat Transfer Symposium, Japan, vol. 3, pp. 752–754 (in Japanese).

Welander, P., 1967. On the oscillatory instability of a differentially heated fluid loop. J. Fluid Mech. 29, 17–30.

Widmann, P.J., Gorman, M., Robbins, K.A., 1989. Nonlinear dynamics of a convection loop 2: chaos in laminar and turbulent flows. Phys. D 36, 157–166.

Yorke, J.A., Yorke, E.D., Mallet-Paret, J., 1987. Lorenz-like chaos in a partial differential equation for a heated fluid loop. Phys. D 24, 279–292.